Changes in Texture and Catalytic Activity of Nanocrystalline MgO during Its Transformation to $MgCl_2$ in the Reaction with 1-Chlorobutane†

Vladimir B. Fenelonov,‡ Maxim S. Mel'gunov,‡ Ilya V. Mishakov,‡ Ryan M. Richards,§ Vladimir V. Chesnokov,‡ Alexander M. Volodin,‡ and Kenneth J. Klabunde*,§

Boreskov Institute of Catalysis, Novosibirsk 630090, Russia, and Department of Chemistry, Kansas State University, Manhattan, Kansas 66506

Received: October 27, 2000; In Final Form: January 9, 2001

The interaction of 1-chlorobutane with nanocrystalline MgO at 200−350 °C has been found to result in both stoichiometric and catalytic dehydrochlorination of 1-chlorobutane to isomers of butene and simultaneous topochemical conversion of MgO to $MgCl_2$. The obtained magnesium chloride appeared to be an active catalyst for the dehydrochlorination reaction, so the rate of 1-chlorobutane conversion grows significantly with time. Changes in the MgO texture during the topochemical reaction are discussed and their effect on the catalytic activity is estimated.

Introduction

Alkaline earth metal (AEM) chlorides and oxides attract significant attention as effective dehydrochlorination catalysts and chemisorbents for many toxic chlorinated organic substances.[1−12] Schematically, the catalytic dehydrochlorination (or generally destructive) reaction (DR) of the AEM chloride with chlorinated compound can be written as

$$MCl_2 + R{-}CH_2{-}CH_2Cl \rightarrow MCl_2 + R{-}CH{=}CH_2 + HCl \quad \text{(I)}$$

and the DR of corresponding oxide as

$$R{-}CH_2{-}CH_2Cl \xrightarrow{MO} R{-}CH{=}CH_2 + HCl$$

$$MO + 2HCl \rightarrow MCl_2 + H_2O \quad \text{(II)}$$

Moreover, both reactions I and II can occur if AEM oxide has been taken as the starting destructive material.

As one can see, comparing with AEM chlorides, DR of corresponding oxides with chlorinated compounds is a more complicated process, which usually results both in the decomposition of the latter and chemical "oxide−chloride" transformation. Usually such DR results in significant changes in the volume of the oxide particles. At the complete transformation the volume of a single MO particle should increase by a factor ∇_{PB}, which is expressed by the Pilling−Bedworth equation:[13,14]

$$\nabla_{PB} = \frac{M_{MCl_2}}{\rho_{MCl_2}} \Big/ \frac{M_{MO}}{\rho_{MO}} \quad (1)$$

Here M and ρ are molecular weight and density of corresponding chloride and oxide. For example, $\nabla_{PB} = 3.64$ for MgO to $MgCl_2$ transformation when $\rho_{MgO} = 3.58$ g/cm^3 and $\rho_{MgCl_2} = 2.32$ g/cm^3 are considered. Such an increase in the volume of the solid phase should result in some changes in the material texture. Both formation of an impermeable coating of $MgCl_2$ over unreacted oxide particles (Figure 1a) and volumetric transformation (Figure 1b) may occur, depending on the exact conditions. Formation of an impermeable coating should not decrease particle dispersion considerably, and thus can result in insignificant changes of material texture. On the contrary, due to a significant shift in the solid-phase volume during volumetric transformation, one can expect decrease in dispersion of particles during transformation. This decrease should be accompanied by decrease in material surface area and pore volume.

Topochemical transformation of conventionally prepared (CP) AEM oxides have been studied already in the literature. However, due to low dispersion, CP oxides usually are not effective in the DRs. As it was recently shown,[1−9] MgO and CaO work most efficiently in the various DRs when their particle size is on the order of nanometers (1−4 nm). Such nanocrystalline oxides can be obtained by the so-called aerogel preparation (AP) technique. These oxides are efficient in DRs due to both high surface area and high concentration of low-coordinated sites and structural defects on their surface.

The present work was devoted to the search for a correlation between the catalytic activity, chemical composition, and morphology of nanoparticles when nanocrystalline MgO samples were subjected to partial conversion to $MgCl_2$ in the reaction with 1-chlorobutane (CB). Special attention was devoted to changes in the texture of the solid phase during the topochemical transformation of MgO to $MgCl_2$.

Experimental Section

Synthesis of Materials. Starting AP−MgO was previously described.[9] In short, AP− AEM oxide was prepared by sequential methoxidation, hydrolysis, hypercritical drying, and heat treatment under vacuum. Thus, clean metal pieces were dissolved in methanol under an inert atmosphere to form metal methoxide, upon vigorous stirring for a few hours, deionized water was added dropwise to form a hydroxide gel, which was dried of solvent in an autoclave and heated under dynamic vacuum to yield the nanometer-sized metal oxide.

Samples with different degrees of AP−MgO conversion to $MgCl_2$ were prepared in the DR with CB at 200, 250, 300, and

† Part of the special issue "John T. Yates, Jr. Festschrift".
* Corresponding author.
‡ Boreskov Institute of Catalysis.
§ Kansas State University.

10.1021/jp0039969 CCC: $20.00 © 2001 American Chemical Society
Published on Web 03/16/2001

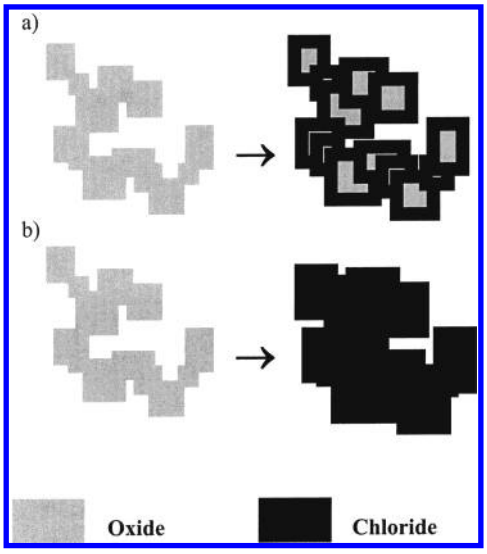

Figure 1. (a) Formation of impermeable chloride coating over oxide nanoparticles. (b) Volumetric transformation of oxide to chloride.

350 °C in a flow reactor with a microbalance. The samples are denoted as *X*-*Z*, where *X* is the reaction temperature and *Z* is the time on-stream in hours. CB vapor was introduced into the reactor in an argon flow at a concentration of 15 vol %. The gas flow rate was 1 L/h, the starting MgO weight was 0.1 g, and the precision of the weight measurement was 10^{-4} g. Prior to the reaction, the samples were activated in an argon flow at 500 °C for 3 h to remove water and other chemisorbed compounds. The composition of the gas after the reactor was determined by gas chromatography. So, the experimental facilities made it possible to control the weight of the sample and the composition of products simultaneously. C_4H_9Cl (99.9%) and argon (99.99%) were used in the experiments.

Methods of Characterization. The actual rate, w_{ACB}, of CB conversion was calculated from its molar concentrations on the inlet and the outlet of the reactor, respectively, and related to the starting MgO weight.

The degree of MgO conversion to $MgCl_2$ (α_{MgO}) was estimated from the weight gain of the sample,with the assumption that the final product consisted only of MgO and $MgCl_2$:

$$\alpha_{MgO} = \frac{m_\alpha - m_{MgO}}{m_{MgCl_2} - m_{MgO}} = \frac{Y_\alpha - 1}{Y_0 - 1} \qquad (2)$$

where m_{MgO} and m_{MgCl_2} are the weights of MgO at the beginning of DR and $MgCl_2$ after complete transformation to chloride, m_α is the weight of the intermediate solid phase (composition of oxide and chloride phases), $Y_\alpha = m_\alpha/m_{MgO}$, and $Y_0 = m_{MgCl_2}/m_{MgO}$. The rate, w_{TR}, of this topochemical reaction in moles per gram of the starting oxide was calculated as $(1/M_{MgO})\, d\alpha_{MgO}/dt$, where *t* is the reaction time. The rate of topochemical reaction is 2-fold lower than the rate, w_{SCB}, of CB stoichiometric conversion. The difference between w_{ACB} and w_{SCB} will be considered further as the rate, w_{CCB}, of catalytic CB conversion:

$$w_{CCB} = w_{ACB} - 2w_{TR} \qquad (3)$$

The isotherms of N_2 adsorption at 77 K were obtained on an ASAP-2400 (Micromeritics, Norcross, GA) installation. Before measurement the samples were heat-treated at 300 °C under dynamic vacuum (2×10^{-3} Torr) for 12 h. The N_2 adsorption isotherms were analyzed by the comparative method.[15,16] The comparative method, based on a comparison of the experimental adsorption isotherm (EI) with a reference adsorption isotherm (RI), is an analogue of a more widely used α_S method.[17] This RI is an averaged curve obtained taking into account numerous adsorption isotherms on various almost nonporous materials of different chemical nature, including nonporous MgO and $MgCl_2$ as well. In a wide region of P/P_0 ($0.1 < P/P_0 < 0.99$), all the isotherms related per surface area of corresponding material, within experimental error, lie on one curve (which is referred here as RI). Reference materials were taken of nonporous materials in order to avoid possible influence of capillary condensation and micropore volume filling effects on RI. Recently the RI was extended in the region of low P/P_0 ($P/P_0 < 0.1$).[18] In ref 18 the possibility of usage of such extended RI for measuring the specific surface areas of silicas was proved. However, the possibility of using the extended RI for materials of a chemical nature different than silica is not proven yet. So, in this study the isotherm reported in refs 15 and 16 was used as RI.

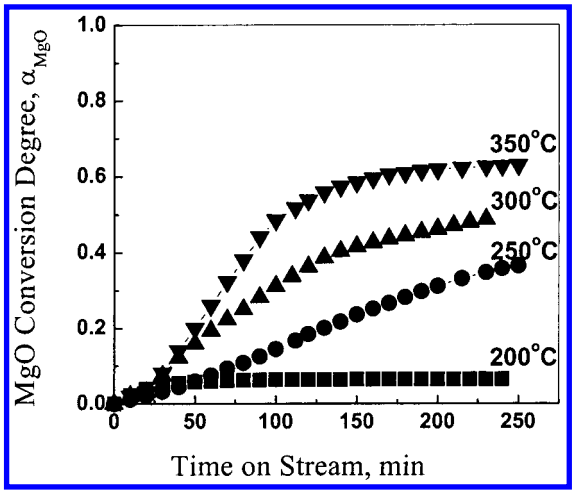

Figure 2. Degree of MgO conversion to $MgCl_2$ during 1-chlorobutane dehydrochlorination over AP−MgO at different temperatures vs time on stream.

Results

According to the results of the chromatographic analysis, the products of CB interaction with MgO include 1-butene and cis and trans isomers of 2-butene in approximately the same amounts. They also contain HCl and water, which were not analyzed quantitatively.

Figure 2 presents time behavior of α_{MgO} at different temperatures. Figure 3 presents the same dependencies of the rate of CB conversion. The rate of the stoichiometric CB conversion is compared with that of the actual CB conversion at 200 °C in Figure 4. One can see that w_{SCB} is terminated at this temperature already at $\alpha_{MgO} = 0.1$ while the conversion of CB goes on. This result indicates that CB dehydrochlorination is mainly a catalytic reaction, which is accelerated by the MgO conversion to $MgCl_2$. At all temperatures the rate of the CB catalytic conversion is significantly higher than that of the stoichiometric reaction at $\alpha_{MgO} > 0.1$. This $\alpha_{MgO} \sim 0.1$ value seems to correspond to full coverage of the surface of MgO particles with a $MgCl_2$ monolayer. At 200 °C the MgO transformation to $MgCl_2$ does not go beyond this point. At higher temperatures both the rate of the catalytic reaction and the degree of the MgO conversion increase considerably. The values of w_{CCB} for different temperatures, calculated from eq 3, are presented in Figure 5.

The $MgCl_2$ formation must be accompanied by changes not only in the stoichiometry of the starting samples but also in

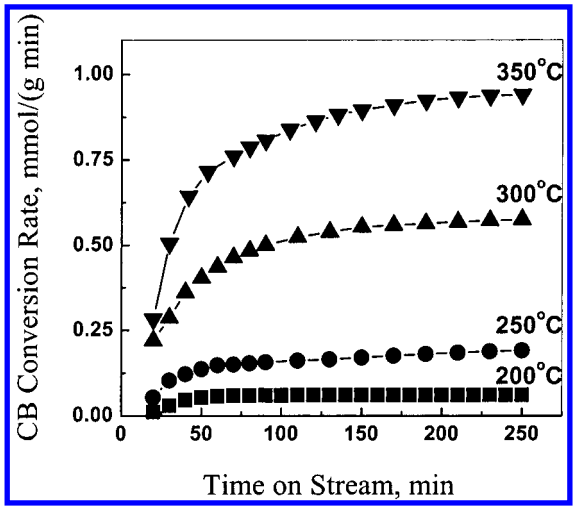

Figure 3. Kinetics of CB conversion at different temperatures.

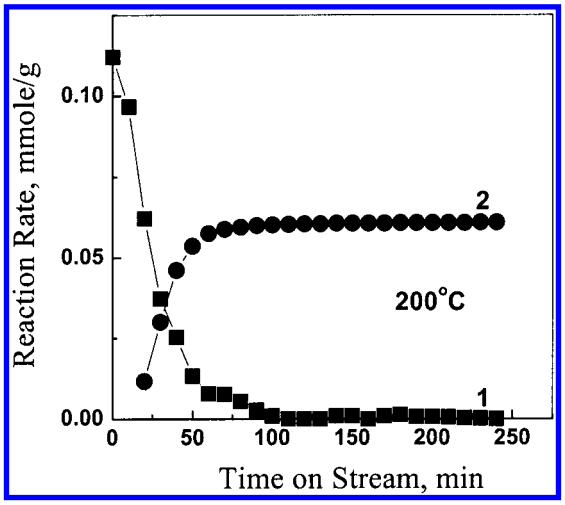

Figure 4. Rates of CB dehydrochlorination over AP−MgO at 200 °C: (1) rate of stoichiometric conversion; (2) actual CB conversion rate.

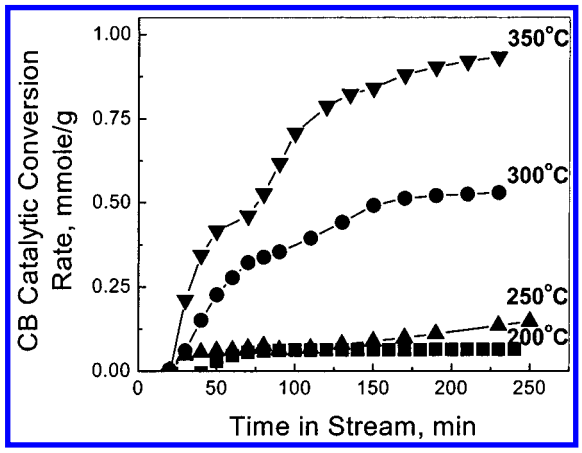

Figure 5. Rates of CB catalytic dehydrochlorination over AP−MgO at different temperatures.

their specific surface area and morphology. Therefore, it is interesting to study textural characteristics of the samples prepared at different α_{MgO} values and evaluate their effect on the chemical reactions.

Changes in the texture resulting from the topochemical reaction were analyzed from the isotherms of nitrogen adsorption at 77 K. As all the isotherms had the same shape, only those obtained on the initial MgO and samples obtained after reaction

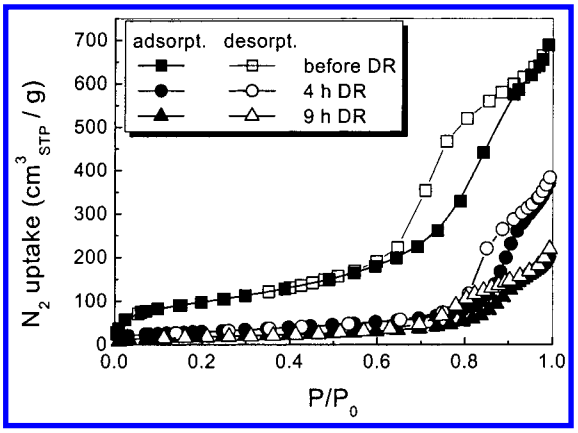

Figure 6. Nitrogen adsorption isotherms for pure AP MgO, after 4 and 9 h of destructive sorption reaction.

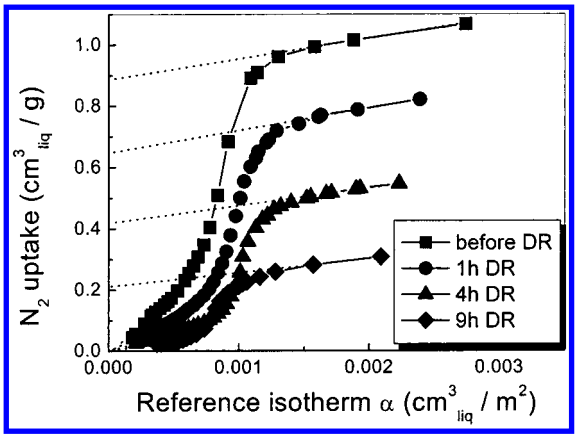

Figure 7. Comparative plots of experimental adsorption isotherms (EI) plotted against a reference isotherm (RI) for pure AP−MgO and after 1, 4, and 9 h of destructive sorption reaction.

at 250 °C are presented in Figure 6 as typical examples. Characteristic loops of the capillary−condensation hysteresis in these adsorption isotherms are typical for systems containing porous aggregates of primary particles. In this case the capillary condensation range corresponds to the filling of the mesopores in the aggregates, while the range above the closure of the hysteresis loop corresponds to polymolecular adsorption on the external surface of such aggregates.

Such interpretation of the isotherms is confirmed by comparative graphs (Figure 7), where the experimental adsorption isotherms (EI) are plotted against a reference isotherm (RI) at the same relative pressures P/P_0. For convenience in the calculations, all adsorption values are expressed in cubic centimeters of liquid nitrogen per gram for EI and per square meter of the surface area for RI. Figure 7 presents comparative plots for initial AP−MgO and samples prepared after reaction at 250 °C. In each curve there are two linear sections separated by a steep ascent. The first linear section at low P/P_0 corresponds to adsorption on the fully accessible surface of the material, i.e., on the surface of primary nonporous nanoparticles. The slope of the dashed line corresponds to the value of full accessible surface area, A. This value is close to the value calculated by the BET method, A_{BET}. For instance, for initial MgO, $A = 373$ m^2/g and $A_{BET} = 355$ m^2/g. The extrapolation of the line to the origin of coordinates indicates the absence of micropores.[15] The steep ascent section corresponds to capillary condensation in mesopores between the primary particles in the aggregates. The second linear section of the curves is located at high P/P_0 values. This linear section corresponds to the region of P/P_0 where adsorption and desorption isotherms join each

TABLE 1: Specific Characteristics of Products Obtained during MgO Transformation to $MgCl_2$[a]

sample	$Y_\alpha = m_\alpha/m_{MgO}$	α_{MgO}	A,[b] m^2/g	A_{ext},[b] m^2/g	V_m,[b] cm^3/g	V_S,[b] cm^3/g	$A_{ext}Y_\alpha$,[c] m^2/g	$V_{ag}Y_\alpha$,[c] cm^3/g
MgO	1.0	0.0	373	72	0.88	1.08	72	1.16
200-1	1.12	0.09	364	68	0.79	1.06	76	1.23
200-4	1.14	0.10	285	66	0.73	0.94	75	1.18
250-1	1.10	0.08	191	70	0.65	0.85	77	1.05
250-4	1.28	0.21	101	56	0.42	0.57	72	0.97
250-5	1.30	0.22	90.2	51	0.37	0.54	66	0.92
250-9	1.62	0.46	72.1	41	0.21	0.33	67	0.97
300-1	1.22	0.16	117	65	0.49	0.68	79	0.99
300-2	1.48	0.35	87.7	53	0.31	0.41	78	1.00
300-3	1.63	0.46	87.6	40	0.25	0.34	65	1.02
350-1	1.24	0.18	114	65	0.61	0.82	80	1.17
350-2	1.71	0.53	41	38	0.11	0.18	65	0.87
350-3	1.98	0.72	42	41	0.08	0.19	81	0.97

[a] Sample names given as (temperature-time in hours online for butyl chloride conversion). α_{MgO} is the degree of MgO conversion to $MgCl_2$. m_α and m_A are the weights of the intermediate solid phase and starting material, respectively. A and A_{ext} are the full and external specific surface areas, respectively. V_m, V_S, and V_{ag} are the volumes of mesopores in aggregates, volume of pores at saturation point ($P/P_0 > 0.99$), and volume of aggregates as a sum of V_m and plus the volume of solid phase, respectively. [b] Values related to the weight of the intermediate product. [c] Values related to the weight of starting MgO.

other, closing the hysteresis loop. In this region of P/P_0, adsorption (and desorption as well) proceeds on the external surface of the porous aggregates of primary nanoparticles without capillary condensation. That allowed us to conclude that the slope of the dashed line in this range is equal to the external surface area, A_{ext}. This line crosses the ordinate axis at the point corresponding to the volume of pores in the aggregates, V_m.

The values of the total specific pore volume measurable by N_2 adsorption, V_S, were calculated from the saturation point at $P/P_S = 0.99$. All basic textural parameters mentioned above are shown in Table 1. Additionally, the surface area of the aggregates $A_{ext}Y_\alpha$ and their volume $V_{ag}Y_\alpha$ as they are related to the weight of the initial MgO are reported. These parameters will be discussed below.

One can see that the α_{MgO} growth always results in a decrease of specific surface area. At the maximum achievable $\alpha_{MgO} \sim 0.5-0.7$, the value of the total surface area A approaches that of the external surface area of the aggregates A_{ext}. The volume of the pores in the aggregates V_m and the total pore volume V_S decrease in the whole range of α_{MgO}. The surface area of the aggregates related to the weight of initial oxide, $A_{ext}Y_\alpha$, is practically independent of α_{MgO}.

Discussion

The above experimental data indicate that type II reaction can account only for the first stage of CB decomposition on AP−MgO. After the formation of $MgCl_2$ coating (see Figure 1a) on the surface of the particles, CB is subjected to catalytic dehydrochlorination. Therefore, the CB interaction with MgO may be considered as a sum of the heterogeneous catalytic reaction on the surface of $MgCl_2$/MgO system (reaction III) and the topochemical reaction on the surface and in the bulk of the solid phase (reaction IV):

$$C_4H_9Cl \rightarrow C_4H_8 + HCl \qquad \text{(III)}$$

Reaction III continues after termination of reaction IV. Correspondingly, HCl formed in reaction III can be either involved in reaction IV or removed into the gas phase.

$$MgO + 2HCl = MgCl_2 + H_2O \qquad \text{(IV)}$$

Let us briefly discuss some features of textural changes during the MgO transformation to $MgCl_2$. The average size of primary MgO nanoparticles, D_{MgO}, evaluated from specific surface area as $D_{MgO} = 6/\rho_{MgO}A_{MgO}$ is equal to 4.5 nm. Complete transformation of such nanoparticles to $MgCl_2$ results in the increase of their volume by a factor of 3.64 as determined from eq 1. Consider the model conditions of MgO transformation to $MgCl_2$, which exclude sintering of individual particles at the places of their contact and the presumably constant number and shape of the particles. For such a model, the relationship of eq 4 between the sizes of $MgCl_2$ and MgO particles must be accurate:

$$D_{MgCl_2} = (\nabla_{PB})^{1/3} D_{MgO} \qquad (4)$$

According to eq 4, D_{MgCl_2} should be equal to 6.9 nm after full transformation. Interestingly, the specific surface area corresponding to such particle size under conditions of the model experiment, $A_{MgCl_2} = 6/\rho_{MgCl_2}D_{MgCl_2} = 374$ m^2/g, is equal to the initial specific surface area of MgO. This similarity should be considered as not regular; however, in this particular case transformation of MgO particles into $MgCl_2$ under conditions excluding sintering of nanoparticles at places of their contacts will not bring noticeable changes in the specific surface area.

Therefore, the experimentally observed decrease of the specific surface area is caused by aggregation of the primary particles with the growth of their size.

The porosity of initial MgO, $\epsilon = V_m\rho_{MgO}/(1 + V_m\rho_{MgO})$, calculated as the ratio of the volume of pores in aggregates to the volume of aggregates, is equal to 0.76. This value corresponds to the average number of contacts per particle[19] $n \approx 2.62/\epsilon = 3.5$. So the low number of contacts appears to be sufficient for significant decrease of specific surface area during transformation.

Among the values reported in Table 1 are those of the surface area of the aggregates $A_{ext}Y_\alpha$, and their volume $V_{ag}Y_\alpha$ related to the weight of initial MgO. They were calculated by the routine described in the Appendix. Obviously, both the volume and the specific surface area of the aggregates are almost independent of temperature and conversion degree. This makes us believe that main bulk transformations caused by the MgO conversion to $MgCl_2$ take place in the bulk of the aggregates without significant changes in their average size determined as a ratio of their volume to their surface area. Hence, the observed changes in the surface area and porosity are primarily caused by the accretion of primary particles inside the aggregates while the dimensions of the aggregates are preserved.

Despite a significant decrease in the specific surface area, the catalytic activity of the samples in dehydrochlorination of CB increases significantly as MgO is converted to $MgCl_2$. The time resolution of the catalytic installation did not allow us to measure the rate of the catalytic reaction on pure MgO as some $MgCl_2$ was formed even after a minimal contact with the feed. Nevertheless, the results obtained bring us to a definite conclusion that the catalytic activity of $MgCl_2$ is significantly higher than that of MgO. This is most likely caused by an increase in the strength of Lewis acid sites on the surface of the catalyst resulting from such transformation.

Conclusion

CB interaction with nanocrystalline MgO at 200−350 °C has been shown to result in its catalytic dehydrochlorination to a mixture of butylenes and topochemical transformation of the catalyst to $MgCl_2$. DR over nanocrystalline MgO samples has exhibited the capability to have the composition and structure of the catalyst manipulated by controlling the conditions of the interaction with CB. It is important that a steady performance of the catalyst is observed only after the formation of the surface chloride phase, and its rate increases as the oxide is converted to chloride. It has been shown that the decrease in the surface area during MgO transformation to $MgCl_2$ in the presence of 1-chlorobutane is due to accretion of primary nanoparticles while the size of their aggregates is preserved. It is very likely that a proper choice of the reaction conditions and application of other halocarbons as reagents will make it possible to synthesize new acid catalysts with high surface area on the basis of AP−MgO. Of special interest is the discovered opportunity for the synthesis of multicomponent catalysts, e.g., $MgO/MgCl_2/MgF_2$, by reaction with molecules containing both chlorine and fluorine atoms. Such systems may have high surface area and unusual catalytic properties in acid−base reactions.

Acknowledgment. The financial support of the Army Research office (grant to K.J.K.) is acknowledged with gratitude.

Appendix

The specific volume of porous aggregates V_{ag} is equal to the sum of the specific volume of pores in the aggregates V_m and specific volume of the solid phase $1/\rho_\alpha$, where ρ_α is the true density of the composite formed at conversion degree α. The value of ρ_α can be determined as a ratio of the weight of the product m_α to its true volume V_α.

By use of eq 2, the product weight m_α at conversion degree α_{MgO} can be expressed as follows:

$$m_\alpha = (1 - \alpha_{MgO})m_{MgO} + \alpha_{MgO}m_{MgO} \quad (5)$$

where $(1 - \alpha_{MgO})m_{MgO}$ is the weight of unreacted MgO and $\alpha_{MgO}m_{MgCl_2}$ is the weight of $MgCl_2$ formed.

The volume of the solid product phase V_α is equal to the sum of volumes of the remaining MgO $[(1 - \alpha_{MgO})m_{MgO}/\rho_{MgO}]$ and that of the formed $MgCl_2$ $(\alpha_{MgO}m_{MgCl_2}/\rho_{MgCl_2})$, where ρ_{MgO} and ρ_{MgCl_2} are the densities of oxide and chloride phases, respectively. Then, the density of the intermediate product ρ_α can be calculated as follows:

$$\rho_\alpha = m_\alpha/V_\alpha = \rho_{MgO}[\alpha_{MgO}(Y_0 - 1) + 1]/[\alpha_{MgO}(\nabla_{PB} - 1) + 1] \quad (6)$$

where ∇_{PB} is the Pilling−Bedworth factor at $\alpha_{MgO} = 1.0$.

References and Notes

(1) Li, Y.-X.; Klabunde, K. J. *Langmuir* **1991**, *7*, 1388.
(2) Li, Y.-X.; Koper, O. B.; Atteya, M.; Klabunde, K. J. *Chem. Mater.* **1992**, *4*, 323.
(3) Koper, O. B.; Lagadic, I.; Volodin, A. M.; Klabunde, K. J. *Chem. Mater.* **1997**, *9*, 2468.
(4) Koper, O. B.; Lagadic, I.; Klabunde, K. J. *Chem. Mater.* **1997**, *9*, 838.
(5) Koper, O. B.; Klabunde, K. J. *Chem. Mater.* **1997**, *9*, 2481.
(6) Klabunde, K. J.; Stark, J. V.; Koper, O. B.; Mohs, C.; Park, D. G.; Decker, S.; Jiang, Y.; Lagadic, I.; Zhang, D. *J. Phys. Chem.* **1996**, *100*, 12142.
(7) Koper, O. B.; Li, Y.-X.; Klabunde, K. J. *Chem. Mater.* **1993**, *5*, 500.
(8) Jiang, Y.; Decker, S.; Mohs, C.; Klabunde, K. J. *J. Catal.* **1998**, *180*, 24.
(9) Richards, R.; Li, W.; Decker, S.; Davidson, C.; Koper, O.; Zaikovskii, V. I.; Volodin, A. M.; Rieker, T.; Klabunde, K. J. *J. Am. Chem. Soc.* **2000**, *122*, 4921.
(10) Noller, H.; Kladnig, W. *Catal. Rev., Sci Eng.* **1976**, *13*, 149.
(11) Beranek, L.; Kraus, M. In *Comprehensive Chemical Kinetics*; Bamford, C. H., Tipper, C. F. H., Eds.; Elsevier: Amsterdam, 1978; Vol. 20, p 263.
(12) Malysheva, L. V. Ph.D. Thesis, Boreskov Institute of Catalysis, Novosibirsk, Russia, 1986.
(13) Pilling, M. B.; Bedworth, R. E. *J. Inst. Met.* **1923**, *1*, 529.
(14) Fenelonov, V. B. *React. Kinet. Catal. Lett.* **1994**, *52*, 367.
(15) Karnaukhov, A. P.; Fenelonov, V. B.; Gavrilov, V. Yu. *Pure Appl. Chem.* **1989**, *61*, 1913.
(16) Fenelonov, V. B.; Romannikov, V. N.; Derevyankin, A. Yu. *Microporous Mesoporous Mater.* **1999**, *28*, 57.
(17) Gregg, S. J.; Sing, K. S. W. *Adsorption, Surface Area and Porosity*, 2nd ed.; Academic Press: London, 1982.
(18) Jaroniec, M.; Kruk, M.; Olivier, J. P. *Langmuir* **1999**, *15*, 5410.
(19) Zagrafskaya, R. V.; Karnaukhov, A. P.; Fenelonov, V. B. *Kinet. Catal.* **1975**, *16*, 1583.